A Relaxed Eddy Accumulation (REA) LOPAP-System for Flux Measurements of Nitrous Acid (HONO)

Lisa von der Heyden[1], Walter Wißdorf[1], Ralf Kurtenbach[1], Jörg Kleffmann[1]

[1] Department of Physical and Theoretical Chemistry, Faculty for Mathematics and Natural Sciences, University of Wuppertal, 42097 Wuppertal, Germany

Correspondence to: Jörg Kleffmann (kleffman@uni-wuppertal.de)

Abstract. In the present study a Relaxed Eddy Accumulation (REA) system for the quantification of vertical fluxes of nitrous acid (HONO) was developed and tested. The system is based on a three-channel-LOPAP instrument, for which two channels are used for the updrafts and downdrafts, respectively, and a third one for the correction of chemical interferences. The instrument is coupled to a REA gas inlet, for which an ultrasonic anemometer controls two fast magnetic valves to probe the two channels of the LOPAP instrument depending on the vertical wind direction. A software (PyREA) was developed, which controls the valves and measurement cycles, which regularly alternates between REA-, zero- and parallel ambient measurements. In addition, the assignment of the updrafts and downdrafts to the physical LOPAP channels is periodically alternated, to correct for differences in the interferences of the different air masses. During the study, only small differences of the interferences were identified for the updrafts and downdrafts excluding significant errors when using only one interference channel. In laboratory experiments, high precision of the two channels and the independence of the dilution corrected HONO concentrations on the length of the valve switching periods were demonstrated.

A field campaign was performed in order to test the new REA-LOPAP system at the TROPOS monitoring station in Melpitz, Germany. HONO fluxes in the range of $-4 \cdot 10^{13}$ molecules m^{-2} s^{-1} (deposition) to $+1.0 \cdot 10^{14}$ molecules m^{-2} s^{-1} (emission) were obtained. A typical diurnal variation of the HONO fluxes was observed with low, partly negative fluxes during night-time and higher positive fluxes around noon. After an intensive rain period the positive HONO emissions during daytime were continuously increasing, which was explained by the drying of the upper most ground surfaces. Similar to other campaigns, the highest correlation of the HONO flux was observed with the product of the NO_2 photolysis frequency and the NO_2 concentration ($J(NO_2) \cdot [NO_2]$), which implies a HONO formation by photosensitized conversion of NO_2 on organic surfaces, like e.g. humic acids. Other postulated HONO formation mechanisms are also discussed, but are tentatively ranked being of minor importance for the present field campaign.

1   Introduction

During the last 25 years, high nitrous acid (HONO) mixing ratios have been observed during daytime under very different environmental conditions pointing to a major contribution of HONO photolysis to the oxidation capacity of the lower atmosphere (Neftel et al., 1996; Zhou et al., 2002a; Kleffmann et al., 2005; Acker et al., 2006; Elshorbany et al., 2009; Villena et al., 2011; Li et al., 2012; Yang et al., 2014; Hou et al., 2016; Lee et al., 2016; Tan et al., 2018; Slater et al., 2020). These high HONO levels can only be explained by strong daytime sources, for which (i) heterogeneous reduction of nitrogen dioxide (NO_2) in the presence of organic photosensitizers (George et al., 2005; Stemmler et al., 2006; 2007; Sosedova et al., 2011; Han et al. 2016a; 2016b; 2017; Yang et al., 2021a), (ii) heterogeneous photolysis of nitric acid/nitrate (Zhou et al., 2003; 2011; Laufs and Kleffmann, 2016; Ye et al., 2016; 2017; Romer et al., 2018; Shi et al., 2021) and (iii) bacterial production of nitrite in soil (Su et al., 2011; Ostwald et al., 2013; Maljanen et al., 2013; Oswald et al., 2015; Scharko et al., 2015; Weber et al., 2015) and/or desorption of adsorbed HONO from soil surfaces during daytime (Donaldson et al., 2014; VandenBoer et al., 2014; 2015) have been identified. In contrast, other proposed sources, like the gas-phase reaction of excited NO_2 with water (Crowley and Carl, 1997; Li et al., 2008; Carr et al., 2009; Amedro et al., 2011), the photolysis of nitro-phenols or similar compounds (Bejan et al., 2006; Yang et al., 2021b) and the gas-phase reaction of $HO_2 \times H_2O$ complexes with NO_2 (Li et al., 2014; 2015; Ye et al., 2015) are of minor importance. Except proposed HONO formation by particle nitrate photolysis (Ye et al., 2016; 2017), mainly ground surface sources have yet been identified in laboratory and field studies to explain atmospheric HONO formation during daytime in the atmosphere (Kleffmann, 2007). This is in good agreement with recent HONO gradient studies during daytime by the MAX-DOAS technique (Garcia-Nieto et al., 2018; Ryan et al., 2018; Xing et al., 2021).

In most field studies, the daytime HONO source strength was determined from HONO levels exceeding theoretical photo-stationary state (PSS) values, for which correlations of the daytime source with the photolysis rate coefficient $J(NO_2)$ or the irradiance and the NO_2 concentration were often observed (Vogel et al., 2003; Su et al., 2008; Elshorbany et al., 2009; Sörgel et al. 2011; Villena et al., 2011; Wong et al., 2012; Lee et al., 2016; Crilley et al., 2016). In these studies, the HONO source is mathematically treated as a gas phase process, despite its heterogeneous origin. Thus, the quantification of the daytime source is erroneous and depends on the height of the measurements above the ground and the vertical mixing of the atmosphere. In addition, the assumed PSS conditions may also not be fulfilled when HONO and its precursors are measured close to their sources (Lee et al., 2013; Crilley et al., 2016).

In contrast, flux measurements are able to give direct information about ground surface production and deposition and are a better tool to quantify ground sources of HONO in the lower atmosphere. Available flux observations indicate different HONO precursors. Harrison and Kitto (1994), Ren et al. (2011) and Laufs et al. (2017) found a relationship of the HONO flux with the NO_2 concentration and also its product with light intensity, which can be explained by the photosensitized conversion of NO_2 on humic acid surfaces (Stemmler et al., 2006). In contrast, for grassland spread with manure upward HONO fluxes could not be explain by an NO_2 driven mechanism (Twigg et al., 2011). For high nitrogen soil content, e.g. after fertilization, up to two orders of magnitude higher HONO fluxes compared to most other studies were recently observed in soil chambers (Xue et al., 2019; Tang et al., 2019). Thus, the latter three studies point to a soil nitrogen driven HONO formation mechanism. In contrast, Zhou et al. (2011) observed a correlation of the HONO flux with adsorbed nitric acid and short wavelength radiation, which was explained by photolysis of nitric acid adsorbed on canopy surfaces. Finally, for flux measurements in a forest clearing dominant formation processes explaining the positive daytime HONO fluxes remained unclear. In the same study at a co-located forest floor, only net HONO deposition was observed at the much lower irradiance levels compared to the forest clearing (Sörgel et al., 2015). The difference could be explained again by a photolytic HONO formation mechanism. In conclusion, based on available HONO flux studies, the origin of the main ground surface daytime HONO source is still controversially discussed.

Nowadays, eddy covariance (EC) is the most commonly applied method to measure fluxes between the surface and the atmosphere. The lack of HONO instruments, however, which are fast and sensitive enough for the EC method, requires the

use of indirect methods like the aerodynamic gradient (AG) method (Harrison and Kitto, 1994; Twigg et al., 2011; Sörgel et al., 2015; Laufs et al., 2017) or the Relaxed Eddy Accumulation method (REA) (Ren et al., 2011; Zhou et al., 2011; Zhang et al., 2012).

In the present study a Relaxed Eddy Accumulation system for the quantification of vertical fluxes of HONO based on the LOPAP technique was developed and tested in the laboratory and in the atmosphere.

2   The REA-Method

Turbulent transport is the most important process for the exchange of energy and trace gases between the ground and the atmosphere. When only slow instruments are available, the REA-method is used to determine fluxes of trace gases, for which air masses are collected and analysed in two channels depending on the sign of the vertical wind (w) (Businger and Oncley, 1990). According to meteorological convention, positive and negative vertical wind directions reflect updrafts and downdrafts, respectively. Controlled by the vertical wind data measured by a 3D anemometer, fast valves are used to separate the different air masses to feed the two channels of the instrument. With a constant sample flow rate, the flux F_c of a trace gas c is calculated according to equation (1) from the mean concentration difference of the two channels $(\overline{c_{up}} - \overline{c_{down}})$, the standard deviation of the vertical wind speed σ_W and a coefficient b_0, which is 0.627 under ideal joint Gaussian distribution of w and c (Wyngaard and Moeng, 1992; Ammann and Meixner, 2002; Sakabe et al., 2014):

(1) $F_c = b_0 \cdot \sigma_w^{30\ Min} \cdot \left(\overline{c_{up}} - \overline{c_{down}} \right) .$

An averaging interval of typically 30 min is chosen to ensure that all eddies of different sizes and frequencies are captured, which contribute to the turbulent transport. Several field studies have shown that, depending on the stability of the atmosphere, the coefficient b_0 deviates from the ideal value and can be in the range of 0.51-0.62 (Baker et al., 1992; Katul et al., 1996; Ammann and Meixner, 2002).

To increase the measured concentration difference and to improve the signal-to-noise ratio, the use of a deadband is recommended (Businger and Oncley, 1990; Oncley et al., 1993). Here, sample air is collected only when the vertical wind speed is outside a defined deadband of the width $\pm w_0$ around zero, while smaller eddies with low energy are not accounted for. Besides decreasing the flux errors, the use of a deadband also conserves the used valves by reducing the valve switching frequency. The half width of the deadband w_0 is determined from the variance of the vertical wind $\sigma_w^{5\ Min}$ during the past 5 min:

(2) $w_0 = K \cdot \sigma_w^{5\ Min} .$

Depending on the turbulence distribution and the concentration of c, K-values in the range 0.5-1 are used. Equation (1) can be reformulated when a deadband is used:

(3) $F_c = b \cdot \sigma_w^{30\ Min} \cdot \left(\overline{c_{up\ (w\ >\ w_0)}} - \overline{c_{down\ (w\ <\ -w_0)}} \right) .$

Often variable b-parameters are calculated for each averaging interval, for which different methods have been developed. By the proxy method, a passive scalar s (e.g. temperature) is measured simultaneously and the flux of this scalar is determined by means of the Eddy Covariance method (see e.g. Aubinet et al., 2000). b_{Proxy} is then calculated as:

(4) $b_{Proxy} = \dfrac{F_s}{\sigma_w^{30\ Min} \cdot \left(\overline{s_{up(w > w_0)}} - \overline{s_{down(w < -w_0)}} \right)} .$

By the proxy method, scalar similarity of the transported scalar s and trace gas c is assumed, which implies a similar transport efficiency for all sizes of eddies. This assumption is, however, not always fulfilled (Ruppert et al., 2006). Alternatively, b_w can be also calculated by the vertical wind statistics (Baker et al., 1992; Baker, 2000):

$$(5) \qquad b_w = \frac{\sigma_w^{30\,Min}}{\left(\overline{w_{up(w > w_0)}} - \overline{w_{down(w < -w_0)}}\right)}.$$

The value of b decreases when using a deadband. Simulation studies of turbulence data have consistently shown that b_{model} is
110   exponentially approaching a limit value when increasing the width of the deadband (Pattey et al., 1993; Katul et al., 1996):

$$(6) \qquad b_{model} = \left(1 - a \cdot \left[1 - e^{\left(-d \cdot \frac{w_0}{\sigma_w}\right)}\right]\right) \cdot b_0.$$

The parameter b_0 describes b without using a deadband and a and d are empirical coefficients ($a = 0.37$ and $d = 1.958$) in the
nonlinear regression model describing b as a function of the normalized half width of the deadband (w_0/σ_W) (Pattey et al.,
1993).

115   To exclude systematic errors in the assignment of the air masses to the two channels, an essential requirement for the
application of equation (3) is a mean vertical windspeed $\overline{w}$ of zero in each averaging interval. This requirement can be violated,
e.g. when the investigated surfaces are not perfectly horizontal, or when the anemometer is not perfectly aligned. This is
corrected for by rotation of the three-dimensional wind data $u, v,$ and w in a right-handed Cartesian coordinate system, which
follows the physical streamlines (double rotation method, see Kaimal and Finnigan, 1994). Using a back-looking moving
120   average window of 5 minutes, the rotation is done immediately during data acquisition.

3   Set-up of the instrument

3.1   Modified LOPAP instrument

For the REA system developed in the present study the LOPAP technique is used, which is explained in detail elsewhere
(Heland et al., 2001; Kleffmann et al., 2002). HONO is sampled in a temperature-controlled stripping coil by a selective
125   reaction with the sampling reagent (R1: 1 g l^{-1} sulfanilamide in 1 N HCl) forming a diazonium salt. In the present study, the
originally recommended sulfanilamide concentration of 10 g l^{-1} (Heland et al., 2001) was significantly reduced leading to an
improved signal stability and a still almost quantitative sampling efficiency of 99.6 % at a gas flow rate of 1.05 l min^{-1} (298.15
K, 101325 Pa) applied in the present study. The sampling efficiency was determined by using a pure HONO source (Villena
and Kleffmann, 2021). The more stable signal is explained by prevention of sulfanilamide crystal formation at the inlet of the
130   stripping coil, especially at low humidity.

The stripping coil is installed in an external sampling unit directly in the atmosphere of interest, by which sampling artefacts
in sampling lines are minimized. The sampling solution is transferred by a 3 m long temperature-controlled reagent line to the
LOPAP instrument, where it reacts with the second reagent (R2: 0.1 g l^{-1} N-(1-naphthyl)-ethylenediamine-dihydrochloride
(NEDA) in water) forming a strongly absorbing azo-dye. The absorbance of the dye is determined by modified Lambert-Beer's
135   law (Heland et al. 2001) in a *liquid-core-waveguide*, which consists of a specific Teflon tube (Teflon AF 2400, 0,6 mm i.d.,
195 cm length) with a lower refractive index (n = 1.29) than the reagents. For the correction of interferences two channels in
series are used. In the first coil, HONO is almost completely sampled in addition to small quantities of interfering species. In
contrast, only the interferences are sampled in the second coil. From the difference of both channels, corrected for the sampling
efficiency, the HONO concentration is determined (Kleffmann and Wiesen, 2008). The interference correction assumes a small
140   sampling efficiency of the interfering species, which was confirmed for many trace gases (Heland et al., 2001; Kleffmann et
al., 2002). In addition, intercomparison with the DOAS technique showed excellent agreement under complex photosmog
conditions in a smog chamber and in the urban atmosphere (Kleffmann et al., 2006).

For the application in a REA system, ideally four channels would be necessary to quantify HONO and interferences in the
updrafts and downdrafts. However, this was not possible in one housing of a standard LOPAP instrument. On the other hand,
145   two separate LOPAP instruments would not fit into the available field rack (see section 3.5) and the setup would become too
bulky for turbulence measurements. Thus, a three channel LOPAP-instrument was developed, in which a double-stripping coil

(channel 1 and 2) is used to probe HONO and interferences in one air mass as explained above. An additional single stripping coil (channel 3) probes the other air mass (see Figure 1 and Figure S1). The measured signal in channel 2 is used for interference correction of both channels 1 and 3, which assumes that the concentrations of the interfering species is almost similar for the updrafts and downdrafts. This was confirmed in all measurements in the ambient atmosphere (see sections 4.1 and 5.1).
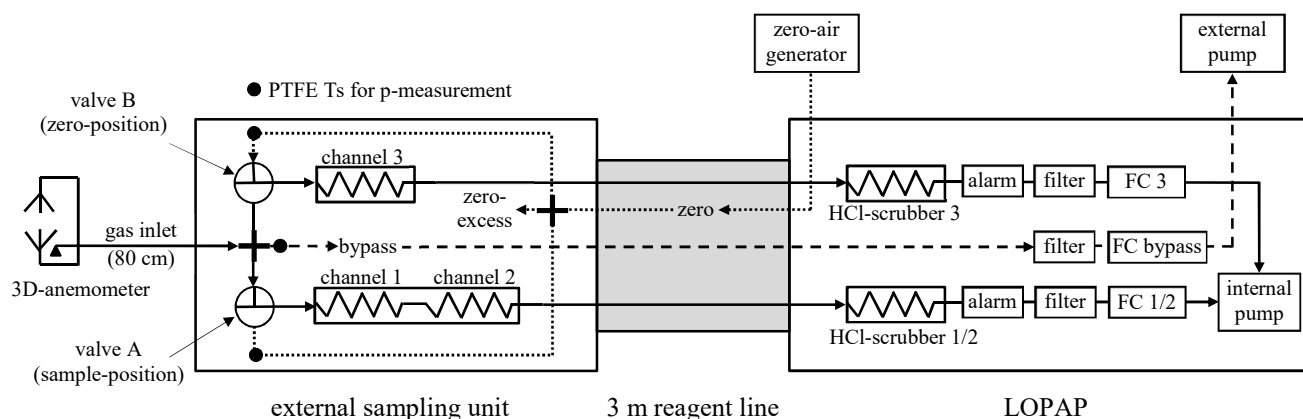
Figure 1: Gas flow scheme of the three-channel REA-LOPAP.

For the additional implementation of the REA gas inlet (see next section) a new compact sampling unit was developed (see Figure S1). In addition, the temperature-controlled reagent line was modified, housing 9 liquid lines for the three channels (see Figure S2) and additional gas lines for the bypass and the zero-gas generator (see Figure 1). In the LOPAP instrument an additional 2 l min^{-1} mass flow controller (Bronkhorst), a second HCl-scrubber and security bottle ("alarm") were installed for the new channel 3. In addition, a 5 l min^{-1} mass flow controller (Bronkhorst) and an external membrane pump (KNF) were installed to control the bypass flow of the REA gas inlet (see Figure 1). Besides, also the liquid flow scheme was adopted to the new 3-channel LOPAP (see Figure S2). Since the internal peristaltic pump (Ismatec) has only 16 channels, from which already 13 are used in a normal 2-channel LOPAP, an additional external 4-channel peristaltic pump was necessary to remove the bubble-containing waste of the three channels from the glass T-junctions behind the stripping coils (see Figure S2).

3.2 The REA gas inlet

For the REA-method two separate channels are probed with updrafts and downdrafts by switching two valves, which are placed in the external sampling unit (see Figure 1 and Figure S1). Caused by its size and to minimize its impact on the turbulence measurements of the ultrasonic anemometer (CSAT3B, Campbell Scientific Inc.) the external sampling unit is installed ~80 cm leeward to the centre of the anemometer (see Figure S4). The ~80 cm long PFA inlet line (4 mm i.d.) from the anemometer to the external sampling unit was covered by aluminium foil to minimize artificial photochemical formation of HONO (Zhou et al., 2002b). The inlet was protected against rain by a small cone (see Figure S4, right; 3 cm diameter) and was positioned below the anemometer, slightly shifted to the lee side, following the recommendations of Kristensen et al. (1997). The use of an inlet line is normally not recommended for the LOPAP technique, but was necessary to spatially separate the anemometer and the external sampling unit. Thus, small positive artefacts could be possible by heterogeneous dark formation of HONO in the inlet. However, this should not affect the HONO fluxes, which are calculated from the concentration difference of updrafts and downdrafts and not from the absolute HONO levels (see equation (3)).

During REA measurements each channel of the instrument is fed for a certain time with ambient air, depending on the vertical wind direction. In contrast, for closed valves, when the vertical wind is too small during deadband conditions or during zero measurements, the LOPAP channels are operated by zero-air. Therefore, fast (<12 ms response time) three-way valves (miniature inert PTFE isolation valves series 1, Parker Hannifin Corp., USA) were used to feed the stripping coils either with ambient air or with zero-air. By using a PTFE cross (BOLA, 1.6 mm i.d.), the sample air from the PFA inlet line is directed to the two valves (see Figure 1 and Figure S1). Since the inlet line has to be flushed by ambient air during the deadband to

minimize heterogeneous HONO formation, the remaining open port of the PTFE cross is connected to the bypass line (see Figure 1 and Figure S1) for which a flow rate of 2.65 l min^{-1} (298.15 K, 101325 Pa) is used in the present study.

The zero-air lines of both channels are connected via a stainless-steel cross (Swagelok, Ohio) to the main zero-gas line. The remaining open port of the cross is used for the excess vent of the zero-air. Zero air was obtained from a home-made zero-air generator (see Figure S4), where compressed ambient air by a membrane pump is pushed through a particle filter, a flowcontroller (Bronkhorst: 5 l min^{-1}), two cartridges filled with active charcoal and active charcoal coated with Na_2CO_3 and another particle filter. The zero-air flow is adjusted slightly higher than the gas flow of both channels, when both valves are closed during deadband and zero-air periods. The dilution of the ambient air during REA measurements is later corrected for during data evaluation (see section 4.1).

During REA-measurements both valves switch between ambient and zero-air. For both measurement conditions a constant air flow through the stripping coil is assumed to correctly calculate the dilution of the ambient air in each channel during the averaging interval. However, constant air flow can only be obtained when the pressure at the inlet of the stripping coil is independent of the valve position. Initially, this was not the case since the pressure at the inlet of the stripping coil was lower during ambient air compared to zero-air measurements. This was caused by the longer inlet line and the higher gas flow rate including sample and bypass flow compared to the flow rate in the shorter zero-air line from the stainless-steel cross (=ambient pressure) to the valve (see Figure 1). Therefore, during first test measurements with variation of the valve switching times (see section 4.2) systematic and significant variations of the resulting dilution-corrected HONO concentrations were observed. Since the flow controllers of the two channels (valve A/channels 1+2; valve B/channel 3) are installed inside the LOPAP instrument and are connected via particle filter, security bottle, HCl-scrubber and a more than 3 m long gas line to the stripping coil (see Figure 1), the flow rates were changing after switching the valves until new pressure equilibria were reached in the volumes from the stripping coil to the flow controller. This problem appeared particularly with short valve switching periods as applied during REA measurements.

To avoid this inlet pressure problem, first, the diameter of the PFA inlet line was increased from initially 1.6 mm i.d. to 4 mm i.d., decreasing the depression at the inlet of the stripping coils. Second, the length of the 1.6 mm i.d. PFA zero lines from the stainless-steel cross (= ambient pressure) to the valves was increased until the pressure at the valve was independent of the valve position (depression similar during ambient and zero-measurements). To adjust the pressure in the REA inlet, three PTFE T-junctions (Bola, 1.6 mm i.d.) were installed at the end of the two zero-air lines at the valves and at the inlet of the bypass line (see Figure 1 and Figure S1). After removing the blind caps from the Ts, the pressure can be measured by a pressure gauge (baratron 0-1000 hPa). For fine adjustment of the pressure, the bypass flow rate is adjusted, which has only an influence on the depression during ambient air measurement, but not during zero-air supply (see Figure 1). For the fine adjustment of the pressure during deadband – here both channels are operated under zero-air and the pressure must be similar at the inlet of both coils – the sample flow rates of both channels were slightly varied. The exact adjustment of the inlet pressures at the two stripping coils under the different operation conditions was the largest problem during the development of the REA-LOPAP system. Only after this was solved, successful REA-measurements were possible.

3.3   REA data logging and valve controlling software - PyREA

Data-logging, processing of the anemometer raw data and control of the REA valves and measurement cycles was performed with a control program, *PyREA*, developed primarily in the *Python* programming language. The applied REA theory and the implemented formula are explained in section 2. Specifically, equation (5) was used to calculate b_w, which is later used to calculate the HONO flux by equation (3). Details of the program are explained in the supplement section S3.

The software was operated on a single board computer (Raspberry Pi, version 3 B+). The user interface of *PyREA* was accessed via a Secure Socket Shell (SSH) connection from the LOPAP data acquisition computer, which allows to control the REA parameters (e.g. mode switching times). Here, the sequence of REA-, zero- and parallel ambient measurements can be adjusted

to run automatically ("auto-REA mode"). During REA measurements, each valve switches between ambient air and zero-air, controlled by the vertical wind signals from the anemometer and the width of the deadband. Regular zero-measurements (both valves are closed) are necessary for the LOPAP technique (Heland et al., 2001) and regular parallel ambient measurements (both valves are open) were used to improve the precision between the two channels for the updrafts and downdrafts.

In the software the different lag times when switching from ambient air measurements to deadband (sample + bypass inlet flow) or from deadband to ambient measurement (only bypass inlet flow) can be adjusted for the REA measurements. Besides the flow rates and the volume of the inlet (10.1 cm^3), also the response time of the valves (12 ms) and the delay of the anemometer (95 ms: only first 10 ms sample of each 100 ms interval is provided by the anemometer) have to be considered. The lag time is calculated by the variable inlet residence time minus the anemometer delay time and the valve response time. Alternatively, the valve can also be operated manually by the graphical interface (GUI), which is necessary during adjustment of the pressure in the REA inlet for example (see section 3.2). Furthermore, different test modes were implemented in the software, which were used during the development of the REA-system. For example, artificial anemometer data can be simulated for tests inside the laboratory (test-mode: *simulate_anemometer*), or the valves can be operated in a pre-defined continuous sequence (test-mode: *valve_function_test*). The latter was used to test the dilution correction for variable valve switching times (see section 4.2).

3.4   Laboratory set-up

To test the new REA-system in the laboratory and in front of the facade of the laboratory building, a mobile laboratory rack was developed, on which all components of the system were installed. The external sampling unit and the anemometer were fixed on an aluminium arm with a similar geometry compared to the field set-up (see Figure S4 left). Through an opening in an exchanged window element of the facade of the laboratory the external sampling unit and the anemometer could be moved outside of the building, while the rack with the LOPAP being inside the laboratory (see Figure S4 right). The opening could be closed by two PVC-plates with smaller holes for the aluminium arm, the insulated reagent line from the external sampling unit to the LOPAP instrument and the cables from the anemometer. This set-up allowed to start measurements inside the laboratory, which was necessary for gas flow rate measurement during calibration for example. Then, with the running instrument the set-up could be changed to ambient test measurements in front of the facade of the building.

3.5   Field set-up in Melpitz

For the field campaign in Melpitz a field rack was available, which was already used in our former gradient measurements in Grignon, France (Laufs et al., 2017). For the present study, the field rack was upgraded with an external air conditioning system with 1 kW cooling power (SoliTherm Outdoor, Seifert Systems GmbH, see Figure S5, left) to ensure constant temperatures inside the rack also under sunny summertime conditions.

The field campaign took place at the field site Melpitz (12.9277° E., 51.5255° N., 86 m NN), which is operated by the TROPOS institute in Leipzig, Germany and is used as a regional station by the Global Atmosphere Watch (GAW) program. The station is located on grass land, which is surrounded by farmland. The nearest buildings of the small village Melpitz are located ~360 m to the east of the station. The terrain is uniform and even, which ensures horizontal homogeneity of the flow field and makes the site well suited for micrometeorological measurements. The railroad tracks from the line Leipzig – Torgau and the state road 87 are located ~1 km and ~1.5 km north of the station, respectively. The next buildings in south-westerly direction are from the village Klitzschen at ~1.5 km distance. A small district road connecting Melpitz and Klitzschen is located ~400 m south of the station. The REA-system was installed ~80 m west of the TROPOS measurement containers and for typical south-westerly winds, no influence of the station on the turbulence and HONO measurements is expected. At ~130 m distance to the west there is a single open line of smaller trees and bushes (see Figure S5, right) with is converging to ~70 m to the south of the field site. The REA-sampling unit and the anemometer were installed on a small mast in south-westerly direction (220°)

to the field rack facing to the expected main wind direction and thus minimizing the influence of the field rack to the turbulence measurements (see Figure S5). The centre of the anemometer was located at ~200 cm height above the grass surface. To avoid
265 turbulence disruptions by the inlet line, the gas inlet was slightly shifted to the lee side (8 cm) and placed below the anemometer at ~170 cm height, following the recommendations of Kristensen et al. (1997). During the campaign, regular parallel ambient measurements of 30 min were used after two measurement cycles (one measurement cycle consists of a 240 min REA period and a subsequent 30 min zero period). As filter for the deadband (see section 2) values of $K = 0.9$ and $K = 0.6$ were used during the campaign.

270 Besides the HONO flux measurements, also the actinic flux and the photolysis frequencies $J(NO_2)$, $J(HONO)$ and $J(O^1D)$ were determined by a spectroradiometer with a cooled CCD detector and a 2π-collector (Meteoconsult) on the roof of one measurement container at the main TROPOS station. In addition, NO- and NO_2-concentrations were measured at the TROPOS station by the chemiluminescence technique (Eco Physics, CLD 770 AL) with blue light NO_2-converter (homemade, University of Wuppertal). The instrument was calibrated six times during the campaign with an NO calibration gas (Messer
275 450±10 ppb) for which also the NO_2 converter efficiency was determined to be (50.4±0.7) % by an O_3-titration unit (Anysco GPT). For the NO_x measurements the common gas inlet of the standard NO_x instrument from the TROPOS station was used, the data of which was not considered here, caused by its higher precision errors and detection limit.

Additionally, data for nitric acid (HNO_3) measured by a MARGA instrument (Stieger et al., 2018), wind-direction and -speed, temperature and relative humidity from the TROPOS station were used for data evaluation.

280 **4   Laboratory tests**

With the laboratory set-up (see section 3.4) test measurements were performed inside the laboratory and at the facade of the laboratory building to develop a data evaluation procedure (section 4.1) and to validate the dilution correction for variable valve switching times (section 4.2).

4.1   Data evaluation

285 During flux measurements simultaneous data from the data acquisition system on the LOPAP computer (HONO raw absorbance) and from the PyREA software on the Raspberry Pi (three-dimensional windspeed (u, v, w), air temperature (T) and valve switching data from the REA inlet) are collected. The software also calculates wind direction and windspeed, as well as the REA parameters b and σ_w.

For both data logging systems 30 s data are recorded, for which the REA data are calculated both, as 5 min and 30 min running
290 averages (see supplement section S3), which are first combined in one data file. Since the time correction of the LOPAP data (lag time between sampling and dye detection) shows a continuous shift caused by a slight reduction of the liquid flow rates of the peristaltic pump, the time-corrected 30 s LOPAP data are synchronized to the 30 s REA data.

The LOPAP data are evaluated similar to the usual procedure (see Heland et al., 2001; Kleffmann et al., 2002). Here, time response (time for 10-90 % increase of the signal: ~5 min) and time correction (time to 50 % change: ~16 min) are determined
295 from the raw data (log(I_{ref}/I), see Heland et al., 2001) and the time stamps of the PyREA software. Furthermore, the raw absorbance of only the zero measurements is described by polynomials as a function of time, which are subtracted from the raw absorbance data, leading to zero-corrected data in the form required by Lambert-Beer's law (log(I_0/I)), which should be zero in between their precision errors during all zero measurements. Next, from the calibration of the instrument by a nitrite standard in R1 (0.01 mg l^{-1}) under zero air, the slopes of the analysis functions (ppt ABS^{-1}) are determined for all three channels,
300 from which the diluted concentrations are calculated by multiplying with the zero-corrected absorbance data (see Figure 2).
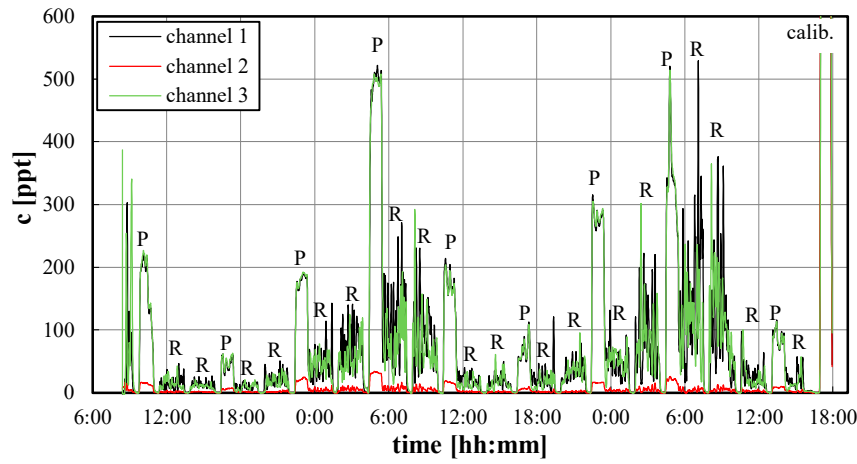
Figure 2: Mixing ratios (30 s raw data) of the three LOPAP channels during test measurements at the university of Wuppertal. Periods named by "P" show undiluted parallel ambient measurements (60 min), while the REA-measurements (dilute samples) are signed by "R" (120 min). In between, regular zero-measurements (30 min) are performed.

305   Since HONO fluxes are determined from small concentration differences between updrafts and downdrafts (see equation (3)), high precision is required for channels 1 and 3. For validation of this requirement, regular parallel ambient measurements are performed by the system, for which both channels measure exactly the same air masses. For the test campaign shown in Figure 2 excellent agreement between both channels was observed for all parallel ambient measurements (periods marked by "P"). In addition, a high correlation of both channels ($R^2 = 0.9986$), excellent agreement (slope: 0.9982 ± 0.0014) and an insignificant

310   intercept of 2 ppt within the quantification error limit were observed. Since the ratio channel 1 / channel 3 showed a small but significant variation with time, the ratio was parameterized as a function of time for later harmonization of both channels (see below).

Next, the concentrations of all three channels were corrected for dilution during the REA-measurements by using the valve switching statistics recorded by the PyREA program for each averaging interval. Depending on the vertical wind direction,

315   each channel of the instrument collects ambient air only for a fraction of the averaging interval (e.g. 1/3). For the rest of the time (i.e. 2/3 for the example), when the instrument is in the dead band, or when the other channel is sampling ambient air, zero air is sucked into the stripping coil. Thus, the measured HONO concentration reflects a diluted sample, with is corrected for by the inverse of sampling fraction (i.e. by multiplication by a factor of 3 in the example). The 5 min moving average data of the valve switching statistics were used for this correction due to the similar physical time response of the LOPAP instrument

320   (see section 3.1). For channels 1 and 2 the valve switching statistics of valve A and for channel 3 the valve switching statistics of valve B were used (see Figure 1).

Then, the dilution-corrected concentrations were harmonized by the parameterization derived from the parallel ambient measurements (see above). Since it is unclear, which of the channels measures correctly, all channels were corrected only by half of the ratio (channel 1 / channel 3) determined during the parallel ambient measurements, for which channels 1 and 2 were

325   divided and channel 3 multiplied by this ratio, respectively. The interference channel 2 was harmonized in the same way than channel 1, since both channels sample the same air mass (see Figure 1). However, caused by the typical small signals in channel 2 (~10 % of channel 1), any errors in the harmonization of channel 2 (typically only 1-2 % correction), will not significantly affect the accuracy of the HONO data (i.e. by only 0.1-0.2 %, much smaller than the precision error of the instrument).

Similar to the usual LOPAP data evaluation (see Heland et al., 2001; Kleffmann et al., 2002), from the corrected and

330   harmonized concentrations in channel 1 and 3 (measuring HONO + interference) the dilution-corrected and harmonized concentrations in channel 2 (measuring only the interference) were subtracted. To consider for the HONO sampling efficiency of the stripping coils, first, the signals of channels 1 and 3 are divided by the sampling efficiency of 0.996 to account for the loss of HONO by incomplete sampling. Second, the loss of HONO to the interference channel 2 (channel 1 × 0.004) is subtracted from channel 2 and only the remaining interference is subtracted from the signals in channel 1 and 3.

335 From the resulting HONO concentrations of both channels an average HONO concentration can be calculated, weighted by the fractions of sampling times of both channels during the 5 min averaging periods (see Figure 3). This average HONO concentration determined by the REA system should be similar to concentrations determined with a normal LOPAP instrument. Deviations caused by missing data during the deadband are considered small, since small concentration differences between the updrafts and downdrafts are expected during the low turbulence deadband conditions. This is confirmed by the

340 non-significant variations of the HONO-concentrations when the system switches from parallel ambient measurements (continuous sampling of ambient air in both channels) to REA-measurements (see Figure 3). Thus, in addition to the HONO fluxes (see below) also HONO concentrations can be determined, similar to a normal LOPAP-instrument. It should be mentioned again that the average HONO concentration determined by the REA-LOPAP system may be affected by systematic artificial HONO formation in the inlet line. However, caused by the high air flow rate of 3.7 l min^{-1} (sum of bypass and sample

345 flow rates of 2.65 l min^{-1} and 1.05 l min^{-1}, respectively) and the short PFA inlet line (80 cm) covered by aluminium foil, artificial heterogeneous HONO formation in the dark inlet during the short residence time of 160 ms is considered small. An intercomparison with a normal LOPAP instrument without any inlet line is required to further confirm this assumption in the future.
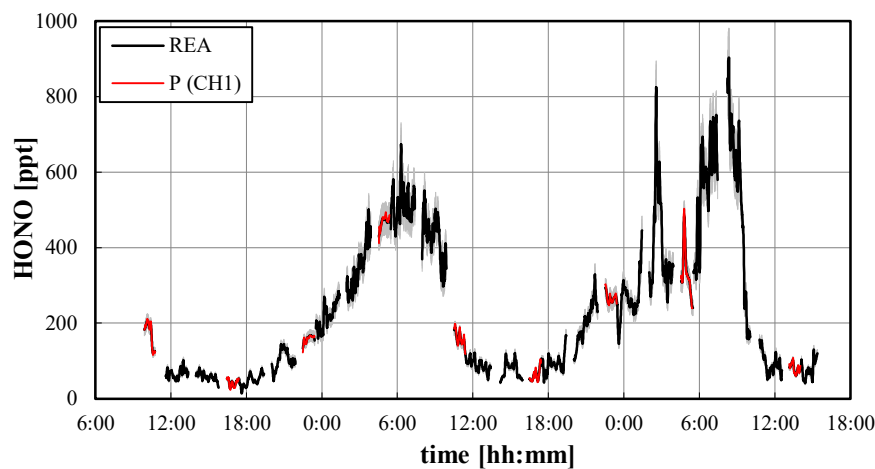
350 **Figure 3: Weighted average HONO concentration determined from both channels during REA measurements (REA) and HONO concentration from channel 1 during parallel ambient measurements (P (CH1)) for the test campaign at the university of Wuppertal (30 s data, 5 min running mean). The grey shaded area reflects the accuracy of the data.**

To validate that the applied interference correction using a three-channel system is applicable, the assignment of the updrafts and downdrafts to the two physical LOPAP channels is regularly alternated after each parallel ambient measurement by the

355 PyREA software. In the mode "up", channels 1 and 2 (double stripping coil) are fed with ascending air and channel 3 (single stripping coil) measures the descending air, while the assignment is inverted in the mode "down". Thus, the relative interference can be determined for both air masses. For the test measurements at the university of Wuppertal average interferences of (8.4±2.4) % and (7.5±4.3) % were determined for the updrafts and downdrafts, respectively. These values are similar within their combined variability. Even if the difference was considered, this would only affect the HONO

360 concentrations in channel 3 by less than ±1 %, which is lower than the precision error. In the case of potential larger differences of interferences in other campaigns, the data from channel 3 could be corrected considering the measured average ratio *interference$_{up}$/ interference$_{down}$* depending on the mode ("up"/"down") applied.

Besides the validation of the interference correction method, the regularly changing assignment of the air masses to the two physical channels of the REA-LOPAP has to be considered for the determination of the HONO flux, which is calculated from

365 the concentration difference of both channels (ΔHONO = HONO$_{up}$ - HONO$_{down}$). Due to the requirement of the REA-method (see section 2) 30 min running means of ΔHONO are calculated. By using the measured ambient pressure and the air temperature ΔHONO is converted from mixing ratios [ppt] to concentrations [molecules m^{-3}]. According to equation (3) (see

section 2) HONO fluxes [molecules m^{-2} s^{-1}] are obtained by multiplication of ΔHONO with 30 min running mean values of b [---] and σ_w [m s^{-1}] obtained from the PyREA software. The fluxes determined during the test measurements in Wuppertal

370   were however not further considered, caused by the distorted turbulence in front of the facade of laboratory building.

4.2   Variation of valve switching periods

After correctly adjusting the pressure in the REA inlet (see section 3.2) the valve switching periods were systematically varied by using the PyREA test-mode *valve_function_test* (see section 3.3) at constant HONO concentrations by using a pure HONO source (Villena and Kleffmann, 2021). A sequence of zero- (both valves closed), parallel ambient measurements (both valves

375   open) and subsequent valve switching periods was performed, for which constant valve switching times of 1, 2, 3 and 4 s were applied for the periodically switching valve positions (1) up, (2) deadband, (3) down and (4) deadband, respectively. Caused by the chosen valve switching sequence, the HONO concentration is diluted exactly by a factor of four in both channels during these experiments (see Figure 4: "P" and "xs").
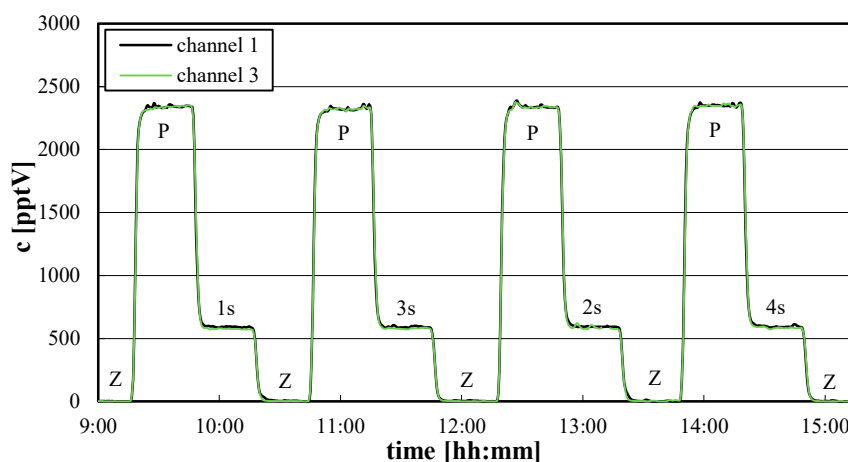
380   **Figure 4: HONO mixing ratios during test measurements using a pure HONO source and variable valve switching times (30 s data). "Z": zero; "P": parallel ambient measurements; "xs": valve switching experiments with constant periods for up-, down and deadband measurements (each with 1, 2, 3, 4 s using the sequence: up, deadband, down and deadband; dilution each by a factor of four).**

For the parallel ambient measurements an excellent agreement between channels 1 and 3 was again observed, with an average

385   ratio (channel 1/ channel 3) of 1.002±0.006. Thus, no further harmonization of the two channels (see section 4.1) was performed for the short measurement period applied. For the valve switching test the expected dilution by a factor of four could be confirmed in both channels. Here, a mean ratio (channel 1 / channel 3) for the dilution corrected data of 1.023±0.012 was observed. The small deviation of 2.3 % is in between the precision error of the instrument considering the applied dilution correction and is independent of the chosen switching time interval. In addition, no significant differences between the HONO

390   data during parallel ambient measurements and the dilution-corrected data during the valve-switching experiments were observed. For the average ratios (parallel ambient measurements / valve switching) values of 0.984±0.015 and 1.005±0.017 were observed for channels 1 and 3, respectively. Thus first, the agreement between both channels is independent of the valve switching period and second, the dilution is correctly determined by the system, which is the basic requirement for REA-measurements.

395   4.3   Flux errors

Errors in the fluxes were determined by error propagation of the accuracy of the LOPAP instrument (7 %), estimated uncertainty in the harmonization function derived from the parallel ambient measurements (5 %), the precision errors of the 30 min values of σ_w / b_w (standard deviation of the 5 min running mean data) and the HONO concentration difference ΔHONO. For the latter the precision of the LOPAP instrument (2.2 % for the campaign in Melpitz), the detection limit (0.8 ppt for the

400 campaign in Melpitz) and the dilution ratios during REA-measurents were considered for all channels of the instrument by error propagation. Possible uncertainties introduced by the choice of calculation method of the *b*-coefficient (see section 2) were not considered in error propagation, but *b*-values determined by different methods were compared to assess their quality (see section 5.1).

Further systematic errors in REA-fluxes can arise from insufficient fulfillment of the prerequisites and assumptions, which

405 underly all micrometeorological flux measurement methods (see e.g. Baldocchi et al., 1988). Therefore, results of field campaigns are often assessed by evaluating turbulence development (see supplement section S7 for the field campaign in Melpitz). Furthermore, the correct determination of the time lag between the change of the sign of the vertical wind and the actual switching of the valves is vitally important for the attribution of the sampled air to the two measurement channels. Imprecise time lags can cause significant errors on determined fluxes, especially in REA systems with long inlet lines (Moravek

410 et al., 2013). The time lags of our system depend mainly on the sample flow rates and were quite short caused by the short inlet line and the high gas flow rate. Due to the different air flow rates in the inlet, different time lags when switching from ambient air to deadband (57 ms) or from deadband to ambient air (123 ms) were individually considered (for details see section 3.3). Therefore, errors of the calculated fluxes caused by imprecise time lags are expected to be negligible for the present application.

415 **5 Field campaign in Melpitz**

5.1 General observations

The field campaign took place during the period 27-09 to 02-10-2020 after a period of strong rain. During the campaign the weather was dry and sunny again, with completely clear sky on the 01-10-2020. The temperatures varied from 3.5 °C during night up to 20 °C during early afternoon. The relative humidity was in the range 50-60 % during early afternoon and increased

420 to 100 % at late night/early morning (see Figure S6). The turbulence was well developed between 8:30 and 16:30 h, while low wind speeds and stable stratification of the atmosphere caused higher relative errors of the HONO fluxes in the evenings and during night-time (see supplement section S7).

Caused by the requirements of the REA-method (see section 2), 30 min averages of the data of all instruments were used for the data evaluation. In addition, only those periods were used for which data from all instruments were available. Besides a

425 short failure of the data logger of the spectroradiometer on the 29-09-2020, during calibrations of the NO_x instrument and during zero and parallel ambient measurements of the LOPAP also no flux data were available. Finally, data with wind directions from north-north-east (340-50°) were also not considered, in order to avoid potential turbulence disturbance of the field rack.

The NO_x concentrations were relatively high for this rural measurement site. NO decreased from up to 12 ppb in the morning

430 to the detection limit of the instrument (30 ppt) in the late afternoon. NO_2 showed smaller variability with mixing ratios in the range 2-10 ppb (see Figure S6). HONO levels varied in the range 2-280 ppt (see Figure 5), but did not show a typical urban diurnal variation with high concentrations during night-time decreasing after sunrise to a minimum in the late afternoon (see for example Figure 3 at the University of Wuppertal). Especially for the 30-09 to 02-10-2020 in Melpitz the HONO concentrations were decreasing during the night and then increased again in the morning with a maximum before noon. Since

435 the NO_x levels were also high at that time (see Figure S6), the late morning peaks may be explained by delayed arrival of polluted air masses, e.g. from the morning rush hour in Leipzig.

Interferences were determined both, for the updrafts and downdrafts by regular changing of the allocation of the air masses to the physical channels of the instrument. Mean values of *interference*$_{up}$ = (7.0±5.5) % and *interference*$_{down}$ = (8.0±7.8) % were determined, which were similar in between their combined variability. In addition, similar concentration dependencies of the

440 interferences were observed, which show decreasing interferences with increasing HONO levels, similar to other LOPAP

measurements (see Figure 5 in Kleffmann and Wiesen, 2008). Thus, the applied interference correction, using the interference data only from one channel for both air masses is considered accurate enough to determine HONO fluxes by the three-channel REA-LOPAP system.

The comparison of three methods for calculation of the *b*-values (see section 2, equations (4) – (6)) during the field campaign in Melpitz using two *K*-values of 0.9 and 0.6 (see equation (2)) showed very good agreement, when data from 08:30 to 16:30 h were used. The average daytime b_w (equation (5)) was 0.35 ± 0.02 for K = 0.9 and 0.43 ± 0.03 for K = 0.6. These values are in good agreement with daytime values of b_{Proxy} determined with the sonic temperature as proxy scalar (see equation (4)) of 0.34 ± 0.06 and 0.38 ± 0.05, respectively. Finally, when a typical experimentally determined value of $b_0 = 0.56$ (Katul et al., 1996; Baker et al., 1992) was used in equation (6), the parameterized b_{model} were 0.36 and 0.39, respectively.
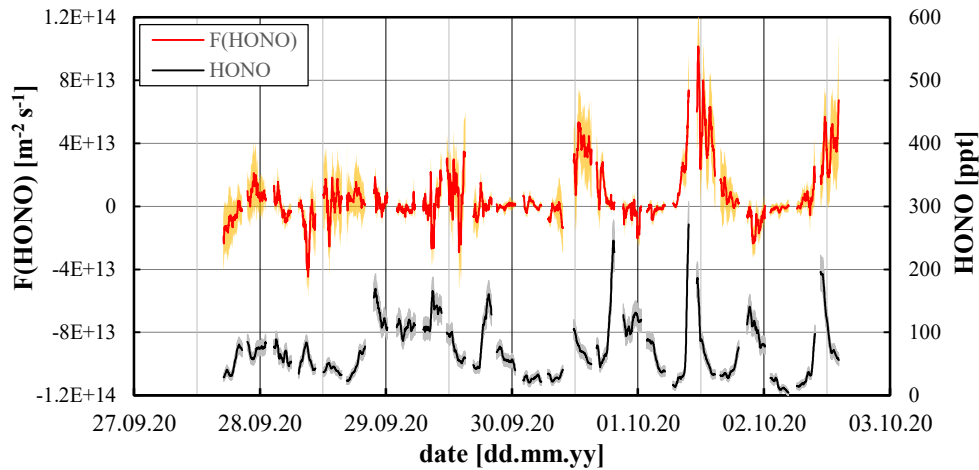
Figure 5: HONO mixing ratios and HONO fluxes (30 min running mean data) in Melpitz. The grey and orange shaded areas reflect the accuracy of the data.

5.2   HONO fluxes

The HONO fluxes showed a clear diurnal trend with low fluxes during night-time and a maximum around noon. The positive daytime fluxes were increasing to the end of the campaign (see Figure 5), which is explained by the previous strong rain period and the slowly drying soil surfaces during the following dry period. Since HONO is well soluble in water – particularly when in contact to slightly alkaline soil surfaces – high HONO emissions were initially prevented by the wet surfaces and increased only when the soil surfaces dried. During the last days a clear diurnal flux profile was observed showing low, partially negative fluxes (deposition) during night-time and higher positive fluxes (emission) around noon. During the campaign, the HONO fluxes varied in the range $-4 \cdot 10^{13}$ to $+1.0 \cdot 10^{14}$ molecules m^{-2} s^{-1} (see Figure 5).

For a better description of the general trends, a mean diurnal profile was calculated from the 30 min mean data of all instruments for the last four days, which is shown in Figure 6. As already described above for the single days, low and partially negative fluxes were observed during night-time, which were increasing to $\sim 4 \cdot 10^{13}$ molecules m^{-2} s^{-1} during daytime around noon.

In other studies, very similar diurnal trends of the HONO flux were observed, which are following the diurnal trend of the radiation (Ren et al., 2011; Zhou et al., 2011; Zhang et al., 2012; Laufs et al., 2017). However, the average maximum HONO fluxes of typically $\sim 1 \cdot 10^{14}$ molecules m^{-2} s^{-1} were higher by factors of 2-3 in these studies compared to the data shown in Figure 6. Only during the BEARPEX 2009 campaign (Ren et al., 2011) and in a forest clearing (Sörgel et al. 2015) lower daytime HONO fluxes were observed compared to the present study. Reasons for the low HONO fluxes in Melpitz may be the solubility of HONO on the wet surfaces, as mentioned above, or lower nitrogen content in the non-fertilized soils of the Melpitz grass land compared to the other studies. In recent flux studies using twin open top soil chambers in China, up to two orders of magnitude higher HONO fluxes were observed shortly after strong fertilization of the soil surfaces (Tang et al., 2019; Xue et al., 2019).
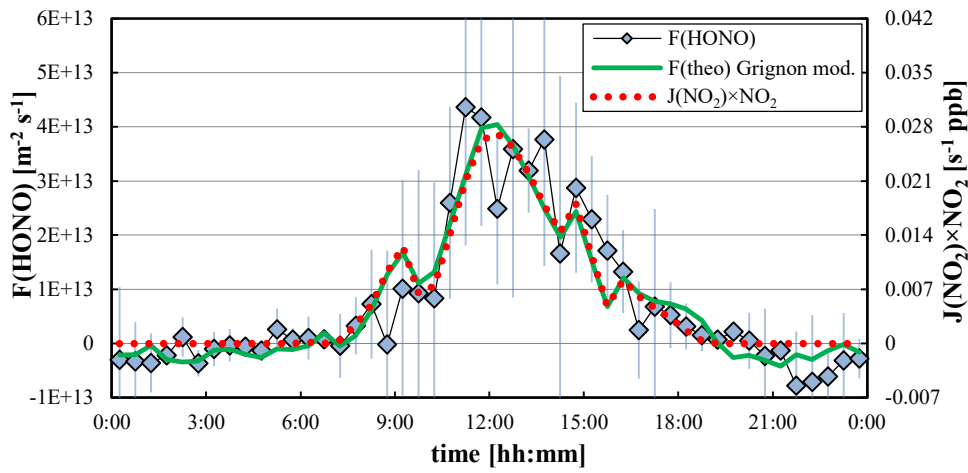
Figure 6: Average diurnal day of the HONO fluxes of the last four days of the campaign in comparison to a modified parameterization from former gradient measurements in Grignon/France (Laufs et al., 2017), see section 5.4. Error bars represent the standard deviation of the HONO fluxes of the four days. In addition, the scaled product $J(NO_2) \cdot [NO_2]$ is also shown.

5.3   Potential HONO formation mechanisms

To identify potential HONO formation mechanisms, the diurnal averaged HONO fluxes were plotted against different potential precursors and parameters. The best correlation was observed between the HONO flux and the product $J(NO_2) \cdot [NO_2]$ (R^2 = 0.86, see also Figure 6), which is in excellent agreement with REA flux measurements during the CalNex 2010 campaign (Ren et al., 2011) and gradient measurements in Grignon/France (Laufs et al., 2017). The results are also in good qualitative agreement with field studies, in which the daytime source of HONO was determined by the photo stationary state (PSS) approach. In these studies, good correlations of the HONO source were observed with radiation (*J(NO₂)* or *irradiance*) and/or the product of *radiation·[NO₂]* (Vogel et al., 2003; Elshorbany et al., 2009; Sörgel et al., 2011; Villena et al., 2011; Wong et al., 2012; Lee et al., 2016; Meusel et al., 2016). These results point to a HONO formation mechanism identified in the laboratory by the photosensitized conversion of NO_2 on organic surfaces, e.g. on humic acids (George et al., 2005; Stemmler et al., 2006; 2007; Bartels-Rausch, 2010; Han et al., 2016a; 2016b; 2017; Yang et al., 2021a).

Based on laboratory and field studies, other HONO sources are also discussed, for example the photolysis of nitrate/HNO_3 adsorbed on surfaces (Zhou et al., 2003; 2011), which requires shorter UV wavelength compared to the photosensitized conversion of NO_2 (see above). Unfortunately, nitrate concentrations on the soil and leaf surfaces were not measured in the present study. However, it is expected that the maximum of this HONO source typically appears in the afternoon, since HNO_3 mainly forms by the oxidation of NO_2 by OH radicals in the gas phase during daytime, followed by the dry deposition of gaseous HNO_3 to ground surfaces. The diurnal maximum of gas phase HNO_3 in the afternoon was confirmed for the present field campaign (see Figure 7) and an even later maximum is expected for deposited HNO_3 on ground surfaces. Since the highest HONO fluxes were observed around noon (Figure 7), main HONO formation by nitrate/HNO_3 photolysis is unlikely for the present field site. In addition, the correlation of the HONO flux with the product $J(O^1D) \cdot [HNO_3]$ (R^2 = 0.60) was weaker compared to the product $J(NO_2) \cdot [NO_2]$ (R^2 = 0.86). Here $J(O^1D)$ was used for the nitrate/HNO_3 photolysis because of the expected similar spectral ranges of the action spectra of HNO_3 and O_3 in the atmosphere (290 – 330 nm). Finally, only low photolysis frequencies $J(HNO_3)$ of adsorbed nitrate/HNO_3 were observed in recent laboratory studies (Laufs et al., 2017; Shi et al., 2021), confirmed by a field study, for which the nitrate photolysis was also excluded as a main HONO source in the atmosphere (Romer et al., 2018).

The microbiological formation of nitrite in soils was proposed in laboratory studies as a further HONO daytime source (Su et al., 2011, Oswald et al., 2013). For this HONO source a strong negative humidity dependence was observed, which was explained by the solubility of HONO in soil water. In addition, the temperature of the upper layer of the soil was identified as

an important parameter, for which the HONO emissions should increase with the soil temperature. Unfortunately, the soil water content and temperature were not measured in the present field campaign. Due to the heat capacity of the soil, it is expected that the diurnal profiles of both parameters follow those of the air temperature and humidity. Since the highest air temperature and lowest relative humidity were observed at 15:00-17:00 h (see Figure 7), the maximum of a potential biological soil source is expected at similar or even later time of the day. In contrast, the highest fluxes were observed around noon near the maximum of the solar radiation (see Figure 6). In addition, low correlations of the HONO fluxes were observed with the inverse of the relative humidity at 1 m height ($R^2 = 0.26$), with the difference (*100 % - RH*) ($R^2 = 0.31$) and with the near ground (1 m) air temperature ($R^2 = 0.46$), again contradicting a main HONO source by microbiological formation of nitrite in the soil. In a field study by the group, which originally proposed the biological source, also a strong correlation of the HONO emissions with radiation was observed and, therefore, could not confirm their former laboratory results (Oswald et al., 2015). A further proposed daytime HONO source is the replacement of night-time adsorbed HONO/nitrite by strong acids on soil surfaces, for example after deposition of HNO_3 (Donaldson et al., 2014; VandenBoer et al., 2014; 2015). However, also this mechanism seems to be not very plausible in the present study because of the main formation mechanism of HNO_3 and its diurnal mixing ratio profile, with a maximum in the late afternoon (see Figure 7). Caused by the subsequent dry deposition of HNO_3, an even later maximum is expected for the HONO source by acid replacement, in contrast to the observed HONO flux profile.

In a very recent study at the same measurement site in Melpitz, HONO emissions by evaporation of nitrite containing dew water was proposed (Ren et al., 2020). The nitrite was explained by the dry deposition and solubility of HONO in dew water during the preceding night, but which could not be confirmed by parallel dew and gas phase measurements. At first glance, this mechanism could be also plausible for the present field study, since the increase of the HONO concentration in the late morning on the 30-09 to 02-10-2020 (see above) appeared at the same time, when the relative humidity decreased from saturation values (100 % RH), indicating the start time of dew evaporation. At the same time also the average HONO fluxes started to increase (see Figure 7). Dew measurements were not available for the present field study to confirm the proposed mechanism, which is however ranked unlikely here, caused by the smaller integrated deposition of HONO during the night compared to the positive daytime fluxes (see Figure 6). Integrated night-time deposition of HONO of only $5.9 \cdot 10^{16}$ molecules m^{-2} was determined for the average day, much smaller than the integrated average daytime HONO emissions of $7.0 \cdot 10^{17}$ molecules m^{-2}. Thus, even when assuming an unreasonable quantitative re-emission of night-time deposited HONO, only at maximum ~8 % of the observed daytime fluxes could be explained by the proposed dew evaporation mechanism, which is thus considered unlikely for the present field campaign. The same quantitative argument is another hint to also exclude the above-mentioned acid replacement mechanism.
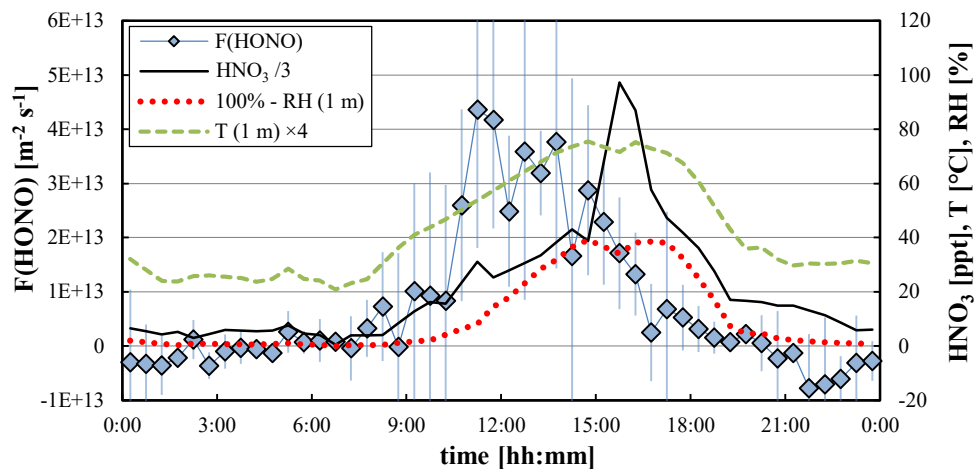
Figure 7: Average diurnal profiles of the HONO flux, HNO₃ mixing ratio and the relative humidity (100%-RH) and temperature of the air in 1 m height. Error bars represent the standard deviation of the HONO fluxes of the four days.

540   For this quantitative comparison the deposition of HONO may underestimate the nitrite levels adsorbed on the ground or in the dew, since nitrite may be also formed by the deposition and heterogeneous conversion of NO_2 on humid surfaces – the main proposed night-time formation mechanism of HONO on ground surfaces. In contrast, any deposition of HONO formed in the gas phase or on particles, would be accounted for by our flux data. Other HONO/nitrite formation mechanisms on ground surfaces (e.g. HNO_3 photolysis, biological production) will be absent or small during night-time. To calculate the maximum

545   nitrite levels accumulated at the end of the night on ground surfaces by heterogenous conversion of NO_2, a reasonable dark reactive uptake coefficient of NO_2 of 10^{-6} (Kurtenbach et al., 2001) was considered. For such a small uptake coefficient, transport limitations will not be significant and would only further decrease the accumulated nitrite. If the average NO_2 concentration during night-time of 4.8 ppb in Melpitz is considered for a 12 h night, at maximum additional $2.35 \cdot 10^{17}$ m^{-2} nitrite could accumulate on the ground surfaces assuming a HONO yield of 50 % (by 2 $NO_2 + H_2O \rightarrow HONO + HNO_3$). Even if

550   an unreasonable quantitative re-emission of the adsorbed nitrite during daytime is assumed, only a third of the observed positive daytime fluxes could be explained by this mechanism. However, a quantitative re-emission of HONO formed by the heterogeneous NO_2 conversion was yet not observed. In the two field studies, which we are aware of by Stutz et al. (2002) and Laufs et al. (2017), only 3 % and 2-4% of the deposited NO_2 was re-emitted as HONO, respectively. This may be explained by additional losses of nitrite on ground surfaces, e.g. by oxidation to nitrate or bacterial conversion. If a more reasonable

555   fraction of re-emitted HONO of 4 % is considered, only 2.7 % of the measured positive HONO fluxes during daytime could be explained by this mechanism. Furthermore, even if one assumes any higher night-time NO_2 uptake and a quantitative re-emission during daytime (both are unlikely), it is very reasonable that the daytime fluxes of HONO by this re-emission mechanism would show a peak in the morning, when the ground surfaces are irradiated by sunlight leading to the evaporation of the dew. This was observed in all studies, where the dew evaporation mechanism was investigated (e.g. He et al., 2006; Ren

560   et al., 2020). In contrast, a re-emission of the adsorbed nitrite, following exactly the diurnal shape of the product of radiation and NO_2 concentration throughout the whole day (see Figure 6), is implausible.

The temporal coincidence of the increasing HONO fluxes with the decreasing relative humidity in the morning and the high correlation with the product $J(NO_2) \cdot [NO_2]$ (see Figure 6) imply HONO formation by photosensitized NO_2 conversion on ground surfaces, but only when the upper most surface layers get dry after the relative humidity is decreasing below saturation

565   values.

Finally, it has to be highlighted, that most of the discussed processes are still speculative due to the missing measured parameters (adsorbed HNO_3/nitrate on soil and grass leaf surfaces, humic acid and nitrite concentrations of the soil, soil humidity and temperature, strong acid deposition, etc.). Thus, the discussed sources could not be quantitatively described here. Main focus of this field campaign were first flux measurements with the new REA-LOPAP system and not the final

570   identification of the most important source and sink processes, which is planned for the future.

5.4   Parameterization of the HONO fluxes

Due to the excellent agreement of the present study with results from former gradient measurements in Grignon/France (Laufs et al., 2017), for which also the highest correlations of the HONO fluxes with the product $J(NO_2) \cdot [NO_2]$ and low nigh-time deposition were observed, similar sources and sinks can be proposed for both rural field sites. In our former study the HONO

575   fluxes were well described by the following parameterization (Laufs et al., 2017):

$$(7) \qquad F(HONO)_{mod} = \left[\left(A \cdot J(NO_2) \cdot c(NO_2) + B \cdot c(NO_2) \right) \cdot exp\left(\frac{\Delta_{sol}H}{R \cdot T_{soil}} \right) - c(HONO) \cdot v(HONO)_T \right] \cdot \frac{RH}{50\%}.$$

The first and most important term in this equation ($A \cdot J(NO_2) \cdot c(NO_2)$) describes the photosensitized conversion of NO_2 during daytime (see above). The second term ($B \cdot c(NO_2)$) is used to parameterize the night-time formation of HONO by heterogeneous conversion of NO_2 on ground surfaces (Arens et al., 2002; Finlayson-Pitts et al., 2003). Because of the solubility of HONO in

580   soil water, both sources were scaled with the temperature by its enthalpy of solvation ($\Delta_{sol}H$). Since the emission of HONO from soil surfaces and not its solubility in water is considered, a positive sign was used for this Arrhenius-term. The next term ($c(HONO) \cdot v(HONO)_T$) considers the temperature dependent deposition of HONO on the ground, which was observed to increase with decreasing temperature (Laufs et al., 2017). Since it can be expected that both, sources and sinks scale with the humidity (Finlayson-Pitts et al., 2003; Stemmler et al., 2006; Han et al., 2016; Su et al., 2011) all terms were finally

585   parameterized by the relative humidity (*RH/50%*).

When using the original parameters from the former study in Grignon (Laufs et al., 2017), but the air temperature (1 m) instead of the soil temperature, a factor of about three higher fluxes were calculated compared to the measurements in Melpitz, which can be explained by the wet surfaces in the present field campaign (see above). To consider the differences between both campaigns, the constants A and B were decreased to $A = 8.807 \cdot 10^5$ m and $B = 1118.4$ m s^{-1}. Other values in equation (7) (see

590   Laufs et al., 2017) were not changed. With this modified parameterization an excellent qualitative and quantitative agreement with the measured fluxes was observed (see Figure 6), indicating that the main source and sink processes identified in Grignon are also active in Melpitz.

6   Conclusion

A Relaxed Eddy Accumulation (REA) system for the quantification of vertical fluxes of nitrous acid (HONO) was developed

595   and tested, which is based on the LOPAP technique. Two fast acting valves are controlled by the sign of the vertical wind speed and feed the sampled gas flow from the updrafts and downdrafts to two LOPAP channels. The developed PyREA software allows controlling measurement cycles, which regularly alternate between REA-, zero- and parallel ambient measurements. Only small differences of the interferences were identified for the updrafts and downdrafts, excluding significant errors when using only one interference channel. In laboratory experiments, high precision of the two channels and

600   the independence of the dilution corrected HONO concentrations on the length of the valve switching periods were demonstrated.

A field campaign at the TROPOS monitoring station in Melpitz, Germany showed campaign averaged diurnal HONO fluxes in the range of $-8 \cdot 10^{12}$ molecules m^{-2} s^{1} (deposition) during night-time increasing to $+4.4 \cdot 10^{13}$ molecules m^{-2} s^{-1} (emission) around noon. The positive HONO emissions during daytime were continuously increasing after an intensive rainy period,

605   which was explained by the drying of the upper most ground surfaces. Similar to other campaigns the highest correlation of the HONO flux was observed with the product $J(NO_2) \cdot [NO_2]$, which implies a HONO formation by photosensitized conversion of NO$_2$ on organic surfaces, like e.g. humic acids.

7   Acknowledgement

The Deutsche Forschungsgemeinschaft (DFG, German Research Foundation) is acknowledged for the financial support under

610   the contract number KL 1392/4-1. We also would like to thank the TROPOS institute and especially Hartmut Herrmann, Gerald Spindler, Achim Grüner and Laurent Poulain for enabling the field campaign at the measurement station in Melpitz, for their continuous and very helpful support during the campaign and for providing the meteorological data and the data for ozone and nitric acid. In addition, we would like to thank Andreas Held for fruitful discussions and for his feedback and advice regarding the REA system. And finally, we would like to thank the two anonymous referees for their helpful comments.

8   References

Acker, K., Möller, D., Wieprecht, W., Meixner, F. X., Bohn, B., Gilge, S., Plass-Dülmer, C., and Berresheim, H.: Strong Daytime Production of OH from HNO$_2$ at a Rural Mountain Site, Geophys. Res. Lett., 33(2), L02809, doi: 10.1029/2005GL024643, 2006.

Amedro, D., Parker, A. E., Schoemaecker, C., and Fittschen, C.: Direct Observations of OH Radicals after 565 nm Multi-Photon Excitation of NO$_2$ in the Presence of H$_2$O, Chem. Phys. Lett., 513(1-3), 12-16, doi: 10.1016/j.cplett.2011.07.062, 2011.

Ammann, C., and Meixner, F. X.: Stability dependence of the relaxed eddy accumulation coefficient for various scalar quantities, J. Geophys. Res. Atmos., 107(D8), 4071, doi: 10.1029/2001JD000649, 2002.

Arens, F., Gutzwiller, L., Gäggeler, H. W., and Ammann, M.: The Reaction of NO$_2$ with Solid Anthrarobin (1,2,10-trihydroxy-anthracene), Phys. Chem. Chem. Phys., 4(15), 3684-3690, doi: 10.1039/b201713j, 2002.

Aubinet, M., Grelle, A., Ibrom, A., Rannik, Ü., Moncrieff, J., Foken, T., Kowalski, A.S., Martin, P.H., Berbigier, P., Bernhofer, Ch., Clement, R., Elbers, J., Granier, A., Grünwald, T., Morgenstern, K., Pilegaard, K., Rebmann, C., Snijders, W., Valentini, R., and Vesala, T.: Estimates of the Annual Net Carbon and Water Exchange of Forests: The EUROFLUX Methodology, Adv. Ecol. Res., 30, 113–175, doi: 10.1016/S0065-2504(08)60018-5, 1999.

Baker, J. M., Norman, J. M., and Bland, W. L.: Field-scale application of flux measurement by conditional sampling, Agric. For. Meteorol., 62(1), 31-52, doi: 10.1016/0168-1923(92)90004-N, 1992.

Baker, J. M.: Conditional sampling revisited, Agric. For. Meteorol., 104(1), 59–65, doi: 10.1016/S0168-1923(00)00147-7, 2000.

Baldocchi, D. D., Hincks, B. B. and Meyers, T.P.: Measuring Biosphere-Atmosphere Exchanges of Biologically Related Gases with Micrometeorological Methods, Ecology, 69(5), 1331-1340, doi: 10.2307/1941631, 1988.

Bartels-Rausch, T., Brigante, M., Elshorbany, Y. F., Ammann, M., D'Anna, B., George, C., Stemmler, K., Ndour, M., and Kleffmann, J.: Humic Acid in Ice: Photo-Enhanced Conversion of Nitrogen Dioxide into Nitrous Acid, Atmos. Environ., 44(40), 5443-5450, doi: 10.1016/j.atmosenv.2009.12.025, 2010.

Bejan, I., Abd El Aal, Y., Barnes, I., Benter, T., Bohn, B., Wiesen, P., and Kleffmann, J.: The Photolysis of Ortho-Nitrophenols: A new Gas Phase Source of HONO, Phys. Chem. Chem. Phys., 8(17), 2028 - 2035, doi: 10.1039/b516590c, 2006.

Businger, J. A., and Oncley, S. P.: Flux Measurement with Conditional Sampling, J. Atmos. Oceanic Technol., 7(2), 349-352, doi: 10.1175/1520-0426(1990)007<0349:FMWCS>2.0.CO;2, 1990.

Carr, S., Heard, D. E., and Blitz, M. A.: Comment on "Atmospheric Hydroxl Radical Production from Electronically Excited NO$_2$ and H$_2$O", Science, 324(5925), 336b, doi: 10.1126/science.1166669, 2009.

Crilley, L. R., Kramer, L., Pope, F. D., Whalley, L. K., Cryer, D. R., Heard, D. E., Lee, J. D., Reed, C., and Bloss, W. J.: On the interpretation of in situ HONO observations via photochemical steady state, Faraday Discuss., 189, 191-212, doi: 10.1039/C5FD00224A, 2016.

Crowley, J. N., and Carl, S. A.: OH Formation in the Photoexcitation of NO$_2$ Beyond the Dissociation Threshold in the Presence of Water Vapor, J. Phys. Chem. A, 101(23), 4178-4184, doi: 10.1021/jp970319e, 1997.

Donaldson, M. A., Bish, D. L., and Raff, J. D.: Soil surface acidity plays a determining role in the atmosphere-terristial exchange of nitrous acid, Proc. Natl. Acad. Sci. U. S. A., 111(52), 18472-18477, doi: 10.1073/pnas.1418545112, 2014.

Elshorbany, Y. F., Kurtenbach, R., Wiesen, P., Lissi, E., Rubio, M., Villena, G., Gramsch, E., Rickard, A. R., Pilling, M. J., and Kleffmann, J.: Oxidation Capacity of the City Air of Santiago, Chile, Atmos. Chem. Phys., 9(6), 2257-2273, doi: 10.5194/acp-9-2257-2009, 2009.

Finlayson-Pitts, B. J., Wingen, L. M., Sumner, A. L., Syomin, D., and Ramazan, K. A.: The Heterogeneous Hydrolysis of NO$_2$ in Laboratory Systems and in Outdoor and Indoor Atmospheres: An Integrated Mechanism, Phys. Chem. Chem. Phys., 5(2), 223-242, doi: 10.1039/B208564J, 2003.

Garcia-Nieto, D., Benavent, N., and Saiz-Lopez, A.: Measurements of atmospheric HONO vertical distribution and temporal evolution in Madrid (Spain) using the MAX-DOAS technique, Sci. Total Environ., 643, 957-966, doi: 10.1016/j.scitotenv.2018.06.180, 2018.

660 George, C., Strekowski, R. S., Kleffmann, J., Stemmler, K., and Ammann, M.: Photoenhanced Uptake of Gaseous NO_2 on Solid Organic Compounds: A Photochemical Source of HONO?, Faraday Discuss., 130, doi: 10.1039/B417888M, 195-210, 2005.

Han, C., Yang, W., Wu, Q., Yang, H., and Xue, X.: Heterogeneous photochemical conversion of NO_2 to HONO on the humic acid surface under simulated sunlight, Environ. Sci. Technol., 50(10), 5017-5023, doi: 10.1021/acs.est.5b05101, 2016a.

665 Han, C., Yang, W., Wu, Q., Yang, H., and Xue, X.: Key role of pH in the photochemical conversion of NO_2 to HONO on humic acid, Atmos. Environ., 142, 296-302, doi: 10.1016/j.atmosenv.2016.07.053, 2016b.

Han, C., Yang, W., Yang, H., and Xue, X.: Enhanced photochemical conversion of NO_2 to HONO on humic acids in the presence of benzophenone, Environ. Pollut., 231(1), 979-986, doi: 10.1016/j.envpol.2017.08.107, 2017.

Harrison, R. M., and Kitto, A.-M. N.: Evidence for a Surface Source of Atmospheric Nitrous Acid, Atmos. Environ., 28(6),
670 1089-1094, doi: 10.1016/1352-2310(94)90286-0, 1994.

He, Y., Zhou, X., Hou, J., Gao, H., and Bertman, S. B.: Importance of Dew in Controlling the Air-Surface Exchange of HONO in Rural Forested Environments, Geophys. Res. Lett., 33, L02813, doi: 10.1029/2005GL024348, 2006.

Heland, J., Kleffmann, J., Kurtenbach, R., and Wiesen, P.: A New Instrument to Measure Gaseous Nitrous Acid (HONO) in the Atmosphere, Environ. Sci. Technol., 35(15), 3207-3212, doi: 10.1021/es000303t, 2001.

675 Hou, S., Tong, S., Ge, M., and An, J.: Comparison of atmospheric nitrous acid during severe haze and clean periods in Beijing, China, Atmos. Environ., 124(B), 199-206, doi: 10.1016/j.atmosenv.2015.06.023, 2016.

Kaimal, J. C., and Finnigan, J. J.: Atmospheric Boundary Layer Flows: Their Structures and Measurements, Oxford University Press, New York, ISBN: 9780195062397, 1994.

Katul, G. G., Finkelstein, P. L., Clarke, J. F., and Ellestad, T. G.: An Investigation of the Conditional Sampling Method Used
680 to Estimate Fluxes of Active, Reactive, and Passive Scalars, J. Appl. Meteorol. Climatol., 35(10), 1835-1845, doi: 10.1175/1520-0450(1996)035<1835:AIOTCS>2.0.CO;2, 1996.

Kleffmann, J., Heland, J., Kurtenbach, R., Lörzer, J., and Wiesen, P.: A New Instrument (LOPAP) for the Detection of Nitrous Acid (HONO), Environ. Sci. Pollut. Res., 9 (special issue 4), 48-54, 2002.

Kleffmann, J., Gavriloaiei, T., Hofzumahaus, A., Holland, F., Koppmann, R., Rupp, L., Schlosser, E., Siese, M., and Wahner,
685 A.: Daytime Formation of Nitrous Acid: A Major Source of OH Radicals in a Forest, Geophys. Res. Lett., 32(5), L05818, doi: 10.1029/2005GL022524, 2005.

Kleffmann, J., Lörzer, J. C., Wiesen, P., Kern, C., Trick, S., Volkamer, R., Rodenas, M., and Wirtz, K.: Intercomparisons of the DOAS and LOPAP Techniques for the Detection of Nitrous Acid (HONO), Atmos. Environ., 40(20), 3640-3652, doi: 10.1016/j.atmosenv.2006.03.027, 2006.

690 Kleffmann, J.: Daytime Sources of Nitrous Acid (HONO) in the Atmospheric Boundary Layer, Chem. Phys. Chem., 8(8), 1137-1144, doi: 10.1002/cphc.200700016, 2007.

Kleffmann, J., and Wiesen, P.: Technical Note: Quantification of Interferences of Wet Chemical HONO LOPAP Measurements under Simulated Polar Conditions, Atmos. Chem. Phys., 8(22), 6813–6822, doi: 10.5194/acp-8-6813-2008, 2008.

695 Kristensen, L., Mann, J., Oncley, S. P., and Wyngaard, J. C.: How Close is Close Enough When Measuring Scalar Fluxes with Displaced Sensors?, J. Atmos. Ocean. Technol., 14(4), 814-821, doi: 10.1175/1520-0426(1997)014<0814:HCICEW>2.0.CO;2, 1997.

Laufs, S., and Kleffmann, J.: Investigations on HONO formation from photolysis of adsorbed HNO_3 on quartz glass surfaces, Phys. Chem. Chem. Phys, 18(14), 9616–9625, doi: 10.1039/C6CP00436A, 2016.

700 Laufs, S., Cazaunau, M., Stella, P., Kurtenbach, R., Cellier, P., Mellouki, W., Loubet, B., and Kleffmann, J.: Diurnal fluxes of HONO above a crop rotation, Atmos. Chem. Phys, 17(11), 6907-6923, doi: 10.5194/acp-17-6907-2017, 2017.

Lee, B. H., Wood, E. C., Herndon, S. C., Lefer, B. L., Luke, W. T., Brune, W. H., Nelson, D. D., Zahniser, M. S., and Munger, J. W.: Urban measurements of atmospheric nitrous acid: A caveat on the interpretation of the HONO photostationary state, J. Geophys. Res. Atmos., 118(21), 12274-12281, doi: 10.1002/2013JD020341, 2013.

705 Lee, J. D., Whalley, L. K., Heard, D. E., Stone, D., Dunmore, R. E., Hamilton, J. F., Young, D. E., Allan, J. D., Laufs, S., and Kleffmann, J.: Detailed Budget Analysis of HONO in Central London reveals a missing daytime source, Atmos. Chem. Phys., 16(5), 2747-2764, doi: 10.5194/acp-16-2747-2016, 2016.

Kurtenbach, R., Becker, K. H., Gomes, J. A. G., Kleffmann, J., Lörzer, J. C., Spittler, M., Wiesen, P., Ackermann, R., Geyer, A., and Platt, U.: Investigations of Emissions and Heterogeneous Formation of HONO in a Road Traffic Tunnel, Atmos.
710 Environ., 35, 3385-3394, doi: 10.1016/S1352-2310(01)00138-8, 2001.

Li, S., Matthews, J., and Sinha, A.: Atmospheric Hydroxyl Radical Production from Electronically Excited NO_2 and H_2O, Science, 319(5870), 1657-1660, doi: 10.1126/science.1151443, 2008.

Li, X., Brauers, T., Häseler, R., Bohn, B., Fuchs, H., Hofzumahaus, A., Holland, F., Lou, S., Lu, K. D., Rohrer, F., Hu, M., Zeng, L. M., Zhang, Y. H., Garland, R. M., Su, H., Nowak, A., Wiedensohler, A., Takegawa, N., Shao, M., and Wahner, A.:
715 Exploring the Atmospheric Chemistry of Nitrous Acid (HONO) at a Rural Site in Southern China, Atmos. Chem. Phys., 12(3), 1497-1513, doi: 10.5194/acp-12-1497-2012, 2012.

Li, X., Rohrer, F., Hofzumahaus, A., Brauers, T., Häseler, R., Bohn, B., Broch, S., Fuchs, H., Gomm, S., Holland, F., Jäger, J., Kaiser, J., Keutsch, F. N., Lohse, I., Lu, K., Tillmann, R., Wegener, R., Wolfe, G. M., Mentel, T. F., Kiendler-Scharr, A., and Wahner, A.: Missing Gas-Phase Source of HONO Inferred from Zeppelin Measurements in the Troposphere, Science,
720 344(6181), 292-296, doi: 10.1126/science.1248999, 2014.

Li, X., Rohrer, F., Hofzumahaus, A., Brauers, T., Häseler, R., Bohn, B., Broch, S., Fuchs, H., Gomm, S., Holland, F., Jäger, J., Kaiser, J., Keutsch, F. N., Lohse, I., Lu, K., Tillmann, R., Wegener, R., Wolfe, G. M., Mentel, T. F., Kiendler-Scharr, A., and Wahner, A.: Response to Comment on "Missing Gas-Phase Source of HONO Inferred from Zeppelin Measurements in the Troposphere", Science, 348(6241), 1326-e, doi: 10.1126/science.aaa3777, 2015.

725 Maljanen, M., Yli-Pirilä, P., Hytönen, J., Joutsensaari, J., and Martikainen, P. J.: Acidic northern soils as a source of atmospheric nitrous acid (HONO), Soil Biol. Biochem., 67, 94-97, doi: 10.1016/j.soilbio.2013.08.013, 2013.

Meusel, H., Kuhn, U., Reiffs, A., Mallik, C., Harder, H., Martinez, M., Schuladen, J., Bohn, B., Parchatka, U., Crowley, J. N., Fischer, H., Tomsche, L., Novelli, A., Hoffmann, T., Janssen, R. H. H., Hartogensis, O., Pikridas, M., Vrekoussis, M., Bourtsoukidis, E., Weber, B., Lelieveld, J., Williams, J., Pöschl, U., Cheng, Y., and Su, H.: Daytime formation of nitrous acid
730 at a coastal remote site in Cyprus indicating a common ground source of atmospheric HONO and NO. Atmos. Chem. Phys., 16(22), 14475-14493, doi: 10.5194/acp-16-14475-2016, 2016.

Moravek, A., Trebs, I., and Foken, T.: Effect of imprecise lag time and high-frequency attenuation on surface-atmosphere exchange fluxes determined with the relaxed eddy accumulation method, J. Geophys. Res. Atmos., 118(17), 10210-10224, doi: 10.1002/jgrd.50763, 2013.

735 Neftel, A., Blatter, A., Hesterberg, R., and Staffelbach, T.: Measurements of Concentration Gradients of HNO_2 and HNO_3 over a Semi-Natural Ecosystem, Atmos. Environ., 30(17), 3017-3025, doi: 10.1016/1352-2310(96)00011-8, 1996.

Oncley, S. P., Delany, A. C., Horst, T. W., and Tans, P. P.: Verification of flux measurement using relaxed eddy accumulation, Atmos. Environ. Part A. General Topics, 27(15), 2417-2426, doi: 10.1016/0960-1686(93)90409-R, 1993.

Oswald, R., Behrendt, T., Ermel, M., Wu, D., Su, H., Cheng, Y., Breuninger, C., Moravek, A., Mougin, E., Delon, C., Loubet,
740 B., Pommerening-Röser, A., Sörgel, M., Pöschl, U., Hoffmann, T., Andreae, M. O., Meixner, F. X., and Trebs, I.: HONO Emissions from Soil Bacteria as a Major Source of Atmospheric Reactive Nitrogen, Science, 341(6151), 1233-1235, doi: 10.1126/science.1242266, 2013.

Oswald, R., Ermel, M., Hens, K., Novelli, A., Ouwersloot, H. G., Paasonen, P., Petäjä, T., Sipilä, M., Keronen, P., Bäck, J., Königstedt, R., Hosaynali Beygi, Z., Fischer, H., Bohn, B., Kubistin, D., Harder, H., Martinez, M., Williams, J., Hoffmann, T., Trebs, I., and Sörgel, M.: A comparison of HONO budgets for two measurement heights at a field station within the boreal forest in Finland, Atmos. Chem. Phys., 15(2), 799-813, doi: 10.5194/acp-15-799-2015, 2015.

Pattey, E., Desjardins, R. L., and Rochette, P.: Accuracy of the relaxed eddy-accumulation technique, evaluated using CO_2 flux measurements, Bound.-Layer Meteorol., 66(4), 341-355, doi: 10.1007/BF00712728, 1993.

Ren, X., Sanders, J. E., Rajendran, A., Weber, R. J., Goldstein, A. H., Pusede, S. E., Browne, E. C., Min, K.-E., and Cohen, R. C.: A Relaxed Eddy Accumulation System for Measuring Vertical Fluxes of Nitrous Acid, Atmos. Meas. Tech., 4(10), 2093-2103, doi: 10.5194/amt-4-2093-2011, 2011.

Ren, Y., Stieger, B., Spindler, G., Grosselin, B., Mellouki, A., Tuch, T., Wiedensohler, A., and Hermann, H.: Role of the dew water on the ground surface in HONO distribution: a case measurement in Melpitz, Atmos. Chem. Phys., 20(21), 13069-13089, doi: 10.5194/acp-20-13069-2020, 2020.

Romer, P. S., Wooldridge, P. J., Crounse, J. D., Kim, M. J., Wennberg, P. O., Dibb, J. E., Scheuer, E., Blake, D. R., Meinardi, S., Brosius, A. L., Thames, A. B., Miller, D. O., Brune, W. H., Hall, S. R., Ryerson, T. B., and. Cohen, R. C: Constraints on Aerosol Nitrate Photolysis as a Potential Source of HONO and NO_x, Environ. Sci. Technol., 52(23), 13738-13746, doi: 10.1021/acs.est.8b03861, 2018.

Ruppert, J., Thomas, C., and Foken, T.: Scalar Similarity for Relaxed Eddy Accumulation Methods, Bound.-Layer Meteorol., 120(1), 39-63, doi: 10.1007/s10546-005-9043-3, 2006.

Ryan, R. R., Rhodes, S., Tully, M., Wilson, S., Jones, N., Frieß, U., and Schofield, R.: Daytime HONO, NO_2 and aerosol distributions from MAX-DOAS observations in Melbourne, Atmos. Chem. Phys., 18(19), 13969-13985, doi: 10.5194/acp-18-13969-2018, 2018.

Sakabe, A., Ueyama, M., Kosugi, Y., Hamotani, K., Hirano, T. and Hirata, R.: Is the empirical coefficient b for relaxed eddy accumulation method constant?, J. Atmos. Chem., 71(1), 79-94, doi: 10.1007/s10874-014-9282-0, 2014.

Scharko, N. K., Schütte, U. M. E., Berke, A. E., Banina, L., Peel, H. R., Donaldson, M. A., Hemmerich, C., White, J. R., Raff, J. D.: Combined Flux Chamber and Genomic Approach Links Nitrous Acid Emissions to Ammonia Oxidizing Bacteria and Archaea in Urban and Agricultural Soil, Environ. Sci. Technol., 49(23), 13825-13834, doi: 10.1021/acs.est.5b00838, 2015.

Shi, Q., Tao, Y., Krechmer, J. E., Heald, C. L., Murphy, J. G., Kroll, J. H., and Ye, Q.: Laboratory Investigation of Renoxification from the Photolysis of Inorganic Particulate Nitrate, Environ. Sci. Technol., 55(2), 854-861, doi: 10.1021/acs.est.0c06049, 2021.

Slater, E. J., Whalley, L. K., Woodward-Massey, R., Ye, C., Lee, J. D., Squires, F., Hopkins, J. R., Dunmore, R. E., Shaw, M., Hamilton, J. F., Lewis, A. C., Crilley, L. R., Kramer, L., Bloss, W., Vu, T., Sun, Y., Xu, W., Yue, S., Ren, L., Acton, W. J. F., Hewitt, C. N., Wang, X., Fu, P., and Heard, D. E.: Elevated levels of OH observed in haze events during wintertime in central Beijing, Atmos., Chem. Phys., 20(23), 14847-14871, doi: 10.5194/acp-20-14847-2020, 2020.

Sörgel, M., Regelin, E., Bozem, H., Diesch, J.-M., Drewnick, F., Fischer, H., Harder, H., Held, A., Hosaynali-Beygi, Z., Martinez, M., and Zetzsch, C.: Quantification of the Unknown HONO Daytime Source and its Relation to NO_2, Atmos. Chem. Phys., 11(20), 10433–10447, doi: 10.5194/acp-11-10433-2011, 2011.

Sörgel, M., I. Trebs, D. Wu, and A. Held: A comparison of measured HONO uptake and release with calculated source strengths in a heterogeneous forest environment, Atmos. Chem. Phys., 15(16), 9237–9251, doi:10.5194/acp-15-9237-2015, 2015.

Sosedova, Y., Rouvière, A., Bartels-Rausch, T., and Ammann, M.: UVA/Vis-Induced Nitrous Acid Formation on Polyphenolic Films Exposed to Gaseous NO_2, Photochem. Photobiol. Sci., 10, 1680-1690, doi: 10.1039/C1PP05113J, 2011.

Stemmler, K., Ammann, M., Donders, C., Kleffmann, J., and George, C.: Photosensitized Reduction of Nitrogen Dioxide on Humic Acid as a Source of Nitrous Acid, Nature, 440(7081), 195-198, doi: 10.1038/nature04603, 2006.

Stemmler, K., Ndour, M., Elshorbany, Y., Kleffmann, J., D'Anna, B., George, C., Bohn, B., and Ammann, M.: Light Induced Conversion of Nitrogen Dioxide into Nitrous Acid on Submicron Humic Acid Aerosol, Atmos. Chem. Phys., 7(16), 4237-4248, doi: 10.5194/acp-7-4237-2007, 2007.

790 Stieger, B., Spindler, G., Fahlbusch, B., Müller, K., Grüner, A., Poulain, L., Thöni, L., Seitler, E., Wallasch, M., and Herrmann, H.: Measurements of PM_{10} ions and trace gases with the online system MARGA at the research station Melpitz in Germany – A five-year study, J. Atmos. Chem., 75, 33-70, doi: 10.1007/s10874-017-9361-0, 2018.

Stutz, J., Alicke, B., and Neftel, A.: Nitrous Acid Formation in the Urban Atmosphere: Gradient Measurements of NO_2 and HONO over Grass in Milan, Italy, J. Geophys. Res., 107 (D22), 8192, doi: 10.1029/2001JD000390, 2002.

Su, H., Cheng, Y. F., Shao, M., Gao, D. F., Yu, Z. Y., Zeng, L. M., Slanina, J., Zhang, Y. H., and Wiedensohler, A.: Nitrous 795 acid (HONO) and its Daytime Sources at a Rural Site during the 2004 PRIDE-PRD Experiment in China, J. Geophys. Res. Atmos., 113(D14), D14312, doi: 10.1029/2007JD009060, 2008.

Su, H., Cheng, Y., Oswald, R., Behrendt, T., Trebs, I., Meixner, F. X., Andreae, M. O., Cheng, P., Zhang, Y., and Pöschl, U.: Soil Nitrite as a Source of Atmospheric HONO and OH Radicals, Science, 333(6049), 1616-1618, doi: 10.1126/science.1207687, 2011.

800 Tan, Z., Rohrer, F., Lu, K., Ma, X., Bohn, B., Broch, S., Dong, H., Fuchs, H., Gkatzelis, G. I., Hofzumahaus, A., Holland, F., Li, X., Liu, Y., Liu, Y., Novelli, A., Shao, M., Wang, H., Wu, Y., Zeng, L., Hu, M., Kiendler-Scharr, A., Wahner, A., and Zhang, Y.: Wintertime Photochemistry in Beijing: Observations of RO_x Radical Concentrations in the North China Plain during the BEST-ONE Campaign, Atmos. Chem. Phys., 18(16), 12391-12411, doi: 10.5194/acp-18-12391-2018, 2018.

Tang, K., Qin, M., Duan, J., Fang, W., Meng, F., Liang, S., Xie, P., Liu, J., Liu, W., Xue, C., and Mu, Y.: A dual chamber 805 system based on IBBCEAS for measuring fluxes of nitrous acid in agricultural fields in the North China Plain, Atmos. Environ., 196, 10-19, doi: 10.1016/j.atmosenv.2018.09.059, 2019.

Twigg, M. M., House, E., Thomas, R., Whitehead, J., Phillips, G. J., Famulari, D., Fowler, D., Gallagher, M. W., Cape, J. N., Sutton, M. A., and Nemitz, E.: Surface/atmosphere exchange and chemical interactions of reactive nitrogen compounds above a manured grassland, Agric. For. Meteorol., 151(12), 1488-1503, doi: 10.1016/j.agrformet.2011.06.005, 2011.

810 VandenBoer, T. C., Markovic, M. Z., Sanders, J. E., Ren, X., Pusede, S. E., Browne, E. C., Cohen, R. C., Zhang, L., Thomas, J., Brune, W. H., and Murphy, J. G.: Evidence for a nitrous acid (HONO) reservoir at the ground surface in Bakersfield, CA, during CALNex 2010, J. Geophys. Res. Atmos., 119(14), 9093-9106, doi: 10.1002/2013JD020971, 2014.

VandenBoer, T. C., Young, C. J., Talukdar, R. K., Markovic, M. Z., Brown, S. S., Roberts, J. M., and Murphy, J. G.: Nocturnal loss and daytime source of nitrous acid through reactive uptake and displacement, Nat. Geosci., 8, 55-60, doi: 815 10.1038/ngeo2298, 2015.

Villena, G., Wiesen, P., Cantrell, C. A., Flocke, F., Fried, A., Hall, S. R., Hornbrook, R. S., Knapp, D., Kosciuch, E., Mauldin III, R. L., McGrath, J. A., Montzka, D., Richter, D., Ullmann, K., Walega, J., Weibring, P., Weinheimer, A., Staebler, R. M., Liao, J., Huey, L. G., and Kleffmann, J.: Nitrous Acid (HONO) during polar spring in Barrow, Alaska: A net Source of OH Radicals?, J. Geophys. Res. Atmos., 116(D14), D00R07, doi: 10.1029/2011JD016643, 2011.

820 Villena, G., and Kleffmann, J.: A Source for the Continuous Generation of Pure and Quantifiable HONO Mixtures, Atmos. Meas. Tech., 15, 627–637, https://doi.org/10.5194/amt-15-627-2022, 2022.

Vogel, B., Vogel, H., Kleffmann, and J., Kurtenbach, R.: Measured and Simulated Vertical Profiles of Nitrous Acid – Part II. Model Simulations and Indications for a Photolytic Source, Atmos. Environ, 37(21), 2957-2966, doi: 10.1016/S1352-2310(03)00243-7, 2003.

825 Weber, B., Wu, D., Tamm, A., Ruckteschler, N., Rodriguez-Caballero, E., Steinkamp, J., Meusel, H., Elbert, W., Behrendt, T., Sörgel, M., Cheng, Y., Crutzen, P. J., Su, H., and Pöschl, U.: Biological Soil Crusts Accelerate the Nitrogen Cycle through large NO and HONO emissions in drylands, Proc. Natl. Acad. Sci. U. S. A., 112(50), 15384-15389, doi: 10.1073/pnas.1515818112, 2015.

Wong, K. W., Tsai, C., Lefer, B., Haman, C., Grossberg, N., Brune, W. H., Ren, X., Luke, W., and Stutz, J.: Daytime HONO Vertical Gradients during SHARP 2009 in Houston, TX, Atmos. Chem. Phys., 12(2), 635-652, doi: 10.5194/acp-12-635-2012, 2012.

Wyngaard, J. C., and Moeng, C.-H.: Parameterizing turbulent diffusion through the joint probability density, Bound.-Layer Meteorol., 60, 1-13, doi: 10.1007/BF00122059, 1992.

Xing, C., Liu, C., Hu, Q., Fu, Q., Wang, S., Lin, H., Zhu, Y., Wang, S., Wang, W., Javed, Z., Ji, X., and Liu, J.: Vertical distributions of wintertime atmospheric nitrogenous compounds and the corresponding OH radicals production in Leshan, southwest China, J. Environ. Sci., 105, 44-55, doi: 10/1016/j.jes.2020.11.019, 2021.

Xue, C., Ye, C., Zhang, Y., Ma, Z., Liu, P., Zhang, C., Zhao, X., Liu, J., and Mu, Y.: Development and Application of a Twin Open-Top Chambers Method to Measure Soil HONO Emission in the North China Plain, Sci. Total Environ., 659, 621-631, doi: 10.1016/j.scitotenv.2018.12.245, 2019.

Yang, Q., Su, H., Cheng, Y., Lu, K., Cheng, P., Gu, J., Guo, S., Hu, M., Zeng, L., Zhu, T., and Zhang, Y.: Daytime HONO Formation in the Suburban Area of the Megacity Beijing, China, Sci. China Chem., 57(7), 1032-1042, doi: 10.1007/s11426-013-5044-0, 2014.

Yang, W., Han, C., Zhang, T.; Tang, N. Yang, H., and Xue, X.: Heterogeneous photochemical uptake of NO_2 on soil surfaces as an important ground-level HONO source, Environ. Pollut., 271, 116289, doi: 10.1016/j.envpol.2020.116289, 2021a.

Yang, W., You, D., Li, C., Han, C., Tang, N., Yang, H., and Xue, X.: Photolysis of Nitroaromatic Compounds under Sunlight: A Possible Daytime Photochemical Source of Nitrous Acid?, Environ. Sci. Technol. Lett., 8, 9, 747–752, doi: 10.1021/acs.estlett.1c00614, 2021b.

Ye, C., Zhou, X., Pu, D., Stutz, J., Festa, J., Spolaor, M., Cantrell, C., Mauldin, R. L., Weinheimer, A., and Haggerty, J.: Comment on "Missing Gas-Phase Source of HONO Inferred from Zeppelin Measurements in the Troposphere", Science, 348(6241), 1326-d, doi: 10.1126/science.aaa1992, 2015.

Ye, C., Gao, H., Zhang, N., and Zhou, X.: Photolysis of Nitric Acid and Nitrate on Natural and Artificial Surfaces, Environ. Sci. Environ., 50(7), 3530-3536, doi: 10.1021/acs.est.5b05032, 2016.

Ye, C., Zhang, N., Gao, H., and Zhou, X.: Photolysis of Particulate Nitrate as a Source of HONO and NO_x, Environ. Sci. Technol., 51(12), 6849-6856, doi: 10.1021/acs.est.7b00387, 2017.

Zhang, N., Zhou, X., Bertman, S., Tang, D., Alaghmand, M., Shepson, P. B., and Carroll, M. A.: Measurements of ambient HONO concentrations and vertical HONO flux above a northern Michigan forest canopy, Atmos. Chem. Phys., 12(17), 8285-8296, doi: 10.5194/acp-12-8285-2012, 2012.

Zhou, X., Civerolo, K., Dai, H., Huang, G., Schwab, J., and Demerjian, K.: Summertime Nitrous Acid Chemistry in the Atmospheric Boundary Layer at a Rural Site in New York State, J. Geophys. Res., 107(D21), 4590, doi: 10.1029/2001JD001539, 2002a.

Zhou, X., He, Y., Huang, G., Thornberry, T. D., Carroll, M. A., and Bertman, S. B.: Photochemical Production of Nitrous Acid on Glass Sample Manifold Surface, Geophys. Res. Lett., 29(14), 1681, doi: 10.1029/2002GL015080, 2002b.

Zhou, X., Gao, H., He, Y., Huang, G., Bertman, S. B., Civerolo, K., and Schwab, J.: Nitric Acid Photolysis on Surfaces in Low-NO_x Environments: Significant Atmospheric Implications, Geophys. Res. Lett., 30(23), 2217, doi: 10.1029/2003GL018620, 2003.

Zhou, X., Zhang, N., TerAvest, M., Tang, D., Hou, J., Bertman, S., Alaghmand, M., Shepson, P. B., Caroll, M. A., Griffith, S., Dusanter, S., and Stevens, P. S.: Nitric Acid Photolysis on Forest Canopy Surface as a Source for Tropospheric Nitrous Acid, Nat. Geosci., 4, 440-443, doi: 10.1038/ngeo1164, 2011.